nature reviews earth & environment

https://doi.org/10.1038/s43017-024-00639-6

Review article

Check for updates

The formation and evolution of the Earth's inner core

Alfred J. Wilson[1], Christopher J. Davies[1], Andrew M. Walker[2], Monica Pozzo[3,4,5,6], Dario Alfè[3,6,7] & Arwen Deuss[8]

Abstract

The growth of the solid inner core from the liquid outer core provides crucial power for generating the geomagnetic field. However, the traditional view of inner core growth does not include the physical requirement that liquids must be supercooled below the melting point before freezing can begin. In this Review, we explore the impact of supercooling the Earth's core on inner core formation, growth and dynamics, and the interpretation of seismic and palaeomagnetic observations. Mineral physics calculations suggest that at least 450 K of supercooling is needed to spontaneously nucleate the inner core. However, when satisfying inferences from geophysical constraints, the maximum available supercooling is estimated at 420 K and more probably <100 K. Supercooling the Earth's core requires that the inner core had at least two growth regimes. The first regime is a rapid phase that freezes supercooled liquids at rates comparable to outer core dynamics (cm yr^{-1}), followed by the second regime that is a traditional in-equilibrium growth phase proportional to the cooling rate of the core (mm yr^{-1}). Future research should seek evidence for rapid growth in the palaeomagnetic and seismic records and the mechanisms that produce deformation texture, particularly those owing to heterogeneous inner core growth, inner core convection, and coupling between freezing and the magnetic field.

Sections

[1]School of Earth and Environment, University of Leeds, Leeds, UK. [2]Department of Earth Sciences, University of Oxford, Oxford, UK. [3]Department of Earth Sciences, University College London, London, UK. [4]Institute for Materials Discovery, University College London East, London, UK. [5]Faculty of Technological & Innovation Sciences, Universitas Mercatorum, Rome, Italy. [6]London Centre for Nanotechnology, Thomas Young Centre, University College London, London, UK. [7]Dipartimento di Fisica "Ettore Pancini", Università di Napoli Federico II, Napoli, Italy. [8]Department of Earth Sciences, Utrecht University, Utrecht, The Netherlands. e-mail: a.j.wilson1@leeds.ac.uk

Key points

• Growth of the inner core provides crucial power for generating the geomagnetic field. The iron-rich liquids of Earth's core are physically required to be supercooled for the solid inner core to first nucleate, but the traditional picture of inner core growth does not consider supercooling of the core.

• Supercooled liquid metals are expected to freeze rapidly upon nucleation, which means that the inner core could have undergone a phase of initial rapid growth in less than 100 years, comparable to the timescale of outer core convection.

• The rapidly grown region could have been at least as large as the innermost inner core (250–700 km radius) and is predicted to host prolonged convection.

• Deformation related to heterogeneous inner core growth and coupling to the dynamo-generated magnetic field are the most probable explanations of observed seismic elastic anisotropy in the inner core.

• The dynamic consequences and palaeomagnetic signature of a rapidly frozen region in the inner core remain unknown.

• Future research should seek to identify the mechanism that initiated inner core growth and to discover the palaeomagnetic and seismological evidence of this event.

Introduction

Despite constituting less than 2% of the planet, Earth's inner core has a crucial role in the Earth system. As the whole planet loses heat to space, the liquid outer core cools and the inner core grows from the centre of the Earth. Growth arises at the centre because the melting point of the alloy of iron, nickel and lighter elements forming the core increases with depth[1]. At the inner core boundary, latent heat is released as the liquid outer core transforms to solid, providing thermal buoyancy[2]. Lighter elements remain in the outer liquid core because they do not fit into the solid lattice, providing chemical buoyancy[3]. These two effects are the dominant power sources for the geodynamo that generates the magnetic field of the Earth in the liquid outer core[2]. Without these power sources, the dynamo might have switched off long ago as is suspected for Mars[4]. The geomagnetic field helps to shield Earth from solar radiation, and so the presence of the inner core is indirectly linked to the surface environment of Earth.

The traditional view of the thermal history of Earth's core and inner core formation is that the entire core was initially liquid and gradually cooled until the temperature at the centre of the core (T_a) equalled the melting point (T_m) of the constituent alloy ($T_m = T_a$, ~5,600–6,200 K, 360 GPa). This traditional view assumes that the solid inner core nucleated at the centre of the Earth the instant that T_a equalled T_m and then began to slowly grow outward[2,5,6] (Fig. 1a). This slow growth is thought to have continued gradually until the present day, when the size of the inner core reached the seismically observed inner core–outer core boundary (1,221 km from the centre of the Earth). The intersection of core temperature and melting temperature at the inner core boundary provides the primary constraint on the present-day core temperature (~5,300–5,900 K (ref. 5), 330 GPa; Fig. 1a). This constraint on core temperature (which arises from the traditional picture of inner core growth) is used to calculate both the thermal structure of the present-day core and the balance of heat flux through the Earth[2]. This traditional view of the thermal history of Earth[7,8] predicts that the inner core began to grow at 500–1,100 Ma (ref. 9), based on thermal evolution models that produce a core cooling rate of about ~100 K Gyr^{-1} (refs. 2,10).

However, the traditional model of inner core growth, and therefore the standard model of the thermal history of Earth, has been shown to be incomplete[7,11]. The traditional view neglects that freezing the first solids of the inner core introduces an interface between the two phases, with an associated energetic penalty[12]. Cooling the core to below its melting point, termed supercooling, is required to overcome this energetic penalty and initiate inner core growth even in the presence of pre-existing solid surfaces. Without pre-existing surfaces, predictions based on classical nucleation theory[12] (Box 1) estimate that 500–1,000 K of supercooling is required to nucleate the inner core[10,13,14]. However, the mineral physics constraints on the profiles of T_a and T_m together with the seismologically determined inner core radius constrain the maximum supercooling that is compatible with geophysical observations to ~400 K (ref. 15). The incompatibility of the required and allowable supercooling suggests that the core should have never cooled enough for any of the inner core to freeze or that a larger than observed inner core should have frozen owing to the extreme cooling required to initiate growth (Fig. 1). The lack of a physical explanation for the existence of the inner core defines the inner core nucleation paradox[11], which comprises contrasting predictions of inner core age and growth history. The resulting links to the palaeomagnetic record, imprinting the change in geomagnetic field intensity associated with inner core nucleation and the persistence of the field since at least 3.5 Ga (ref. 16), and seismological evidence of inner core structure, controlled by inner core growth and deformation, are therefore also unexplained. Relating these observations to inner core properties and processes requires a coherent model of deep Earth thermal history that incorporates supercooling.

In this Review, we explore the range of viable supercooling estimates that are consistent with first-order observations of the long-term thermal history of Earth. We review the available constraints on supercooling from previous mineral physics and geodynamic models and incorporate these estimates into coupled core–mantle thermal history models. A key implication of these models is a period of rapid initial inner core growth. We discuss the probable growth rate, its geodynamic implications, and its potential expression in the palaeomagnetic record. Finally, we compare the seismically observed structure of the inner core and its inferred dynamics with thermal histories that include supercooling. Future research should focus on identifying the mechanism by which the inner core nucleated, and modelling the freezing of the inner core from supercooled liquids, including the palaeomagnetic and seismological expressions of this growth.

Nucleation of the inner core

Geophysical observations of the deep Earth provide clues as to how much the liquid core might have been supercooled below its melting temperature before inner core nucleation. The mechanism by which the inner core might have nucleated provides constraints on the supercooling required to first freeze solids in the liquid core. In this section, we compare the amount of supercooling compatible with observations and mineral physics calculations.

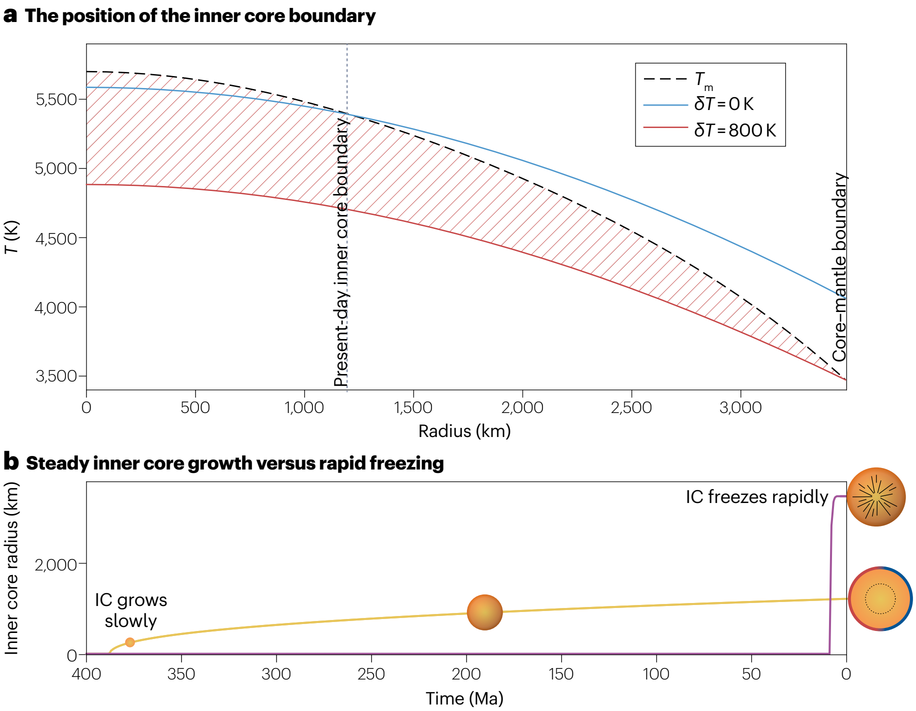

Fig. 1 | The implications of supercooling on inner core growth. a, The intersection of core melting temperature (dashed curve) and adiabat (solid curves) defines the position of the inner core boundary. Cooling the core far below its melting temperature (red curve) before inner core nucleation requires that most of the core was below its melting point (hatched area). **b**, Two scenarios of inner core radius growth over time. The orange case shows a traditional view wherein no supercooling is required and the inner core grows slowly under a single, steady growth regime. The rapid and late-stage growth scenario (purple curve) represents the case when the required supercooling to spontaneously nucleate the inner core (δT) is achieved, causing all supercooled liquid to rapidly freeze. A δT value of 800 K is needed to freeze the inner core[10,11,13], but this high δT value results in a larger than observed inner core size, most of which froze in the past 100 Myr. Supercooling is required to freeze the inner core, but the required δT is incompatible with present-day observations of inner core size. IC, inner core.

Supercooling of the Earth's core

Estimates of the supercooling required to trigger the nucleation of the inner core can be separated into those that are inferred from geophysical observations, such as the size of the inner core, and those that use mineral physics calculations (Fig. 2). Mineral physics calculations assess the necessary conditions to overcome the free-energy barrier defined by nucleation theory (Box 1).

Three different approaches have been used to infer the maximum allowed supercooling from geophysical observations. The most direct are derived by equating the core temperature T_a and melting temperature T_m at the present inner core boundary radius of 1,221 km. Assuming that the inner core froze in the immediate past requires that the whole inner core volume is supercooled with the maximum supercooling arising at the centre of the Earth[10,11,13–15] (Supplementary Fig. 1). Exploring a range of T_m and T_a curves, an upper bound to δT is estimated to be 420 K (ref. 15), although this estimate does not consider the effect of latent heat release on freezing the inner core, which might increase the estimated maximum δT by ~50 K (Fig. 2). Thermal history models that do include this latent heat are discussed later in the Review. The second approach[17] uses two-phase flow modelling to argue that trapping at most 10% liquid in the inner core (as suggested by Singh[18] using seismic observations) requires that the inner core nucleated at no more than half its present size, which implies that δT might not be greater than ~100 K. Finally, correlations of enhanced seismic scattering in the bottom 420–720 km of the inner core with a rapid growth phase could suggest that δT is ~25–70 K (ref. 19), although this constraint relies on the assumption that the observed seismic scattering results from the presence of melt in the inner core. By contrast, observational constraints on the thermal structure of the core and the minimum amount of melt in the inner core (0%) are compatible with a minimum δT of 0 K. Thus, geophysical observations constrain the maximum δT in the range 0–420 K.

Nucleation pathways

Calculations based on mineral physics have also been used to estimate the supercooling required to nucleate solids at the centre of the Earth via homogeneous and heterogeneous nucleation. The assessment of the required supercooling to homogeneously nucleate the inner core began with investigation of pure Fe. Extrapolation of thermodynamic properties[11] determined at lower P and T, simulations of the freezing process[10] and simulations of nucleation kinetics[13] all suggest that pure Fe requires between 730 K and 1,000 K of supercooling to observe a nucleation event in a volume equal to the current inner core within 1 Gyr. A metastable body centred cubic phase of pure Fe might provide a favourable route to freezing, needing only $\delta T = 470$ K, before eventually relaxing to the stable hexagonally close packed phase[14]. Other simulations of nucleation have identified defect-rich crystal structures[13], indicating the assumption of classical nucleation theory (CNT) that the most stable phase will be the first to form, wherein the difference between the chemical potential of solid and liquid $\delta\mu$ is greatest, is not correct. However, simulations still predict that large δT (~500–800 K) is needed and are well described by CNT despite this discrepancy.

The introduction of alloying elements alters the picture of homogeneous nucleation. Oxygen, carbon, silicon and sulfur are all candidate light elements to be present in the iron–nickel core owing to their cosmochemical abundance and partitioning behaviour at core formation conditions. Oxygen and carbon are expected to partition strongly to the liquid iron upon inner core freezing[20,21], whereas silicon and sulfur partition approximately evenly between solid and liquid[22]. Each of these commonly considered light elements has a distinct effect on the energetics of nucleation. Oxygen not only reduces the energy associated with homogeneously forming nuclei ΔG^{hom} but also depresses the melting point of the alloy such that the two effects counteract, resulting in a similar degree of supercooling being needed for spontaneous freezing[10]. Carbon has a similar effect on ΔG^{hom} but depresses

Box 1 | Classical nucleation theory and the inner core nucleation paradox

The inner core nucleation paradox arises from the way that a liquid transforms to a solid as it cools through its melting temperature. Below the melting temperature, the free energy of the solid is lower than the free energy of the same amount of liquid. Although the sign of this energetic term means that the formation of the solid from the liquid would be favoured, in the absence of pre-existing surfaces, some energy is required to form a solid–liquid interface. Until this energy barrier is overcome, the liquid state can persist even below the melting point, when a system is supercooled. The size of the barrier decreases as the system is cooled further below the melting temperature. This supercooling effect is observed in the atmosphere where water droplets persist in the liquid state below the freezing point, until they meet a solid surface such as when snow forms around dust particles or ice flash-freezes on aircraft wings[155]. These examples also illustrate the importance of heterogeneous nucleation, wherein a pre-existing solid reduces the energy barrier and allows rapid freezing.

Classical nucleation theory describes the way the energy barrier to nucleation evolves with temperature[12]. The key idea is that the difference in chemical potential between a solid and a liquid, $\delta\mu$, is released as energy when the supercooled liquid transforms into a solid. This quantity is proportional to the volume of solid and becomes more favourable as the temperature drops further below the melting temperature. However, there is also an energy penalty, γ, associated with the interface that is proportional to the interface area and is typically independent of temperature. This penalty means that for any supercooling, there is a critical radius for nucleation.

The total energy of a homogeneous system ΔG^{hom} decreases if the solid particles that are smaller than this radius melt or if solid particles larger than this radius grow. The energy barrier ΔG^{hom} associated with forming a solid particle of the critical radius, r_c, is then

$$\Delta G^{hom} = \frac{4}{3}\pi r_c^3 \delta\mu + 4\pi r_c^2 \gamma \quad (3)$$

The critical radius gets smaller as the temperature drops. To estimate a waiting time, τ_w, for solidification, the arrangement of atoms in the liquid can be imagined as continually fluctuating as small solid clusters of atoms, with a structure like the solid, continually form and disappear. Nucleation occurs once a cluster larger than the critical radius spontaneously forms (it turns out that the waiting time for this event to occur decreases exponentially with decreasing critical radius), according to:

$$\tau_w = \tau_0 \exp\left(\frac{\Delta G^{hom}(r_c)}{k_B T}\right) \quad (4)$$

where τ_0 is a system-specific kinetic pre-factor and k_B is the Boltzmann constant.

For negligible supercooling, implied by traditional thermal history models of the core, the waiting time is longer than the age of Earth, even for the vast volume concerned. For waiting time shorter that the age of Earth, the supercooling is so large that the whole core would be below its melting temperature, and so it would be entirely solid.

the melting point of iron less than oxygen, leading to a reduction in the required supercooling[15]. A carbon concentration in the core of 5 mol% reduces the required supercooling in the core to 612(±139) K. However, concentrations this high are difficult to reconcile with partitioning and isotopic data[23] and accretionary modelling[24]. Silicon and sulfur both have a negative effect on the nucleation barrier[15] and require greater supercooling than the pure case, needing 1,224(±345) K and 1,821(±1,116) K, respectively, to nucleate the inner core homogeneously with 1 mol% of solute.

Heterogeneous nucleation of iron on a pre-existing surface in the liquid core might offer a marked reduction to the interfacial energy associated with freezing solids. One simple model of heterogeneous nucleation is described by CNT[12] as

$$\Delta G^{het} = f(\theta)\Delta G^{hom}, \text{ with } f(\theta) = \frac{2 - 3\cos\theta + \cos^3\theta}{4} \quad (1)$$

where θ is the wetting or contact angle of the nucleating phase on the pre-existing surface, which reduces the energy barrier ΔG^{hom} by a factor $f(\theta)$ (where $\theta \leq \pi$). This approximation assumes that the pre-existing surface is flat and that greater affinity of the nucleating phase to this surface is described by lower wetting angles (wherein the same volume of nucleated material is spread more thinly over a larger area).

Although heterogeneous nucleation provides an attractive solution to the inner core nucleation paradox, its key assumption (the existence of a pre-existing solid facilitating nucleation of the inner core at modest supercooling) is difficult to justify. One possibility is that solid material was delivered to the early core from impacted planetesimals; however, this material is not expected to survive melting before reaching the innermost liquid core[11]. A second possibility involves sourcing a metallic phase from subducted mantle material collecting at the core mantle boundary. Diamond inclusions suggest that metallic phases are present in the deep mantle[25] and both gold and copper would provide a dense, high melting temperature phase that might sink as diapirs toward the supercooled region of the core. This possibility has been considered, but it was concluded that the core would dissolve such a 'nugget' before it would reach the centre of the Earth[11]. A final possibility arises from the strongly temperature-dependent solubility of the core. Liquid iron is an efficient solvent at the temperatures arising during core formation (~5,000–6,000 K)[26,27], but subsequent cooling reduces the solubility of dissolved elements, potentially causing some fraction to precipitate at the coolest region of the outer core. However, this exsolution mechanism is problematic for three reasons. First, the phase will inevitably be low density compared to the bulk core and so will not easily be mixed into the supercooled region that first forms at the centre of the core. Second, solubility is strongly temperature dependent[9,26,28,29], which means that precipitates will form at the core mantle boundary, furthest from the first supercooled liquids. Third, oxides, which have so far been the most commonly considered precipitates[9,28,30,31], have poor wetting angles for metals[32], which means that they do not tend to sufficiently reduce the nucleation barriers that have been evaluated thus far. A resolution to these issues would be a dense metallic phase with a high melting temperature, which might either have survived accretion or precipitated at high temperature and pressure. A basic ab initio calculation of the forced dissociation of tungsten (W) and carbon in liquid iron reveals a lower energy configuration when the species are dissolved rather than bonded, eliminating the possibility of a tungsten carbide phase in the core (Supplementary Note 2). Ultimately, each of these mechanisms could offer the possibility of a resolution to the inner core nucleation paradox, but none have so far been proven effective at sufficiently reducing the energetic barrier to nucleation (Supplementary Note 3).

Despite the lack of a thermodynamic resolution to the inner core nucleation paradox, the existence of the inner core is indisputably established by geophysical observations, and so a resolution must be possible. One approach is to search for a mechanism from mineral physics that yields a required supercooling that is compatible with geophysical observations. For example, a smaller required supercooling could lie in a hitherto unidentified difference between core nucleation and the predictions of CNT, such as the combined effects of multiple light elements, or a previously unrecognized type of solid that could have facilitated nucleation. A second potential resolution arises from noting that nucleation is random and that existing estimates of the required δT to produce the inner core do not preclude its existence but instead suggest that nucleation was highly improbable and that the Earth could be a rare case. Whatever the resolution, thermal histories of the deep interior of Earth must predict a plausible cooling rate that is consistent with continuous magnetic field generation over the last 3.5 Gyr and the correct present-day inner core size. We now turn to this problem and show that these variables provide another independent constraint on the viable supercooling.

A range of geophysical observations constrain the maximum supercooling at the centre of the Earth to be between 0 and 420 K. By contrast, mineral physics calculations viewed through the lens of CNT suggest that the core should have been supercooled by 600–1,000 K to initiate homogeneous nucleation.

Inner core cooling and growth

A complete thermal history model of inner core evolution describes the thermal state of the deep Earth through time. In this section, we describe an established numerical model of the coupled core and mantle, which includes adaptations to account for supercooling of the liquid core before inner core nucleation. This thermal history model is used to explore the inner core growth rate from a supercooled state. We first focus on long-term (from 4.5 Ga to the present day) core–mantle thermal history, wherein the initial rapid phase of inner core growth can be ignored, before returning to consider the initial growth in the supercooled region.

Inner core growth rate

The existence of a nucleation barrier suggests that the inner core has grown under at least two regimes[17,19]: one regime is immediately after a successful nucleation event wherein all liquid in the supercooled region freezes, and another regime is the traditional picture wherein the inner core boundary tracks the core melting point (Fig. 1). The rate g at which the supercooled region of the liquid core crystallized is not known but is estimated to vary between 0 at T_m (because the driving force $\delta\mu = 0$ at T_m) and a theoretical maximum growth rate g_0 as[33]

$$g = g_0\left(1 - \exp\frac{-\delta\mu(P,T,x)}{RT}\right) \qquad (2)$$

where R is the gas constant and $\delta\mu$ is the difference in chemical potential between the solid and liquid that depends on pressure P, temperature T and composition x. Molecular dynamics simulations[34] suggest that for Ni at ambient pressure, g increases by 0.2 m s^{-1} K^{-1} from 0 at T_m. Simulations of binary iron alloy nucleation[15] at inner core conditions suggest $g = 280$ m s^{-1} at 4,000 K, which means a gradient with respect to T of 0.07 m s^{-1} K^{-1}. These estimates agree with experimental results indicating that crystal growth has close to zero activation energy beyond a critical size in supercooled liquids[35].

Dendritic crystal growth occurs when metals rapidly freeze. These branching crystals can trap residual liquids during growth, making liquid inclusions highly relevant to any rapid growth phase of the inner core. Latent heat release and chemical partitioning will decrease the growth rate predicted by equation (2), but g is still expected to be much faster than the approximately million-year timescale for evolution of the well-mixed core.

Inner core nucleation and growth

Using an established thermal history model[7,8], the effects of supercooling on inner core growth can be explored. This 1D parameterization of coupled core–mantle evolution uses energy balances to calculate changes in mantle and core temperature over geological time[8,36,37], and it predicts key deep Earth properties including the inner core growth rate, long-term variations of magnetic field intensity, and heat transport. The mantle model is a classic plate tectonic parameterization using

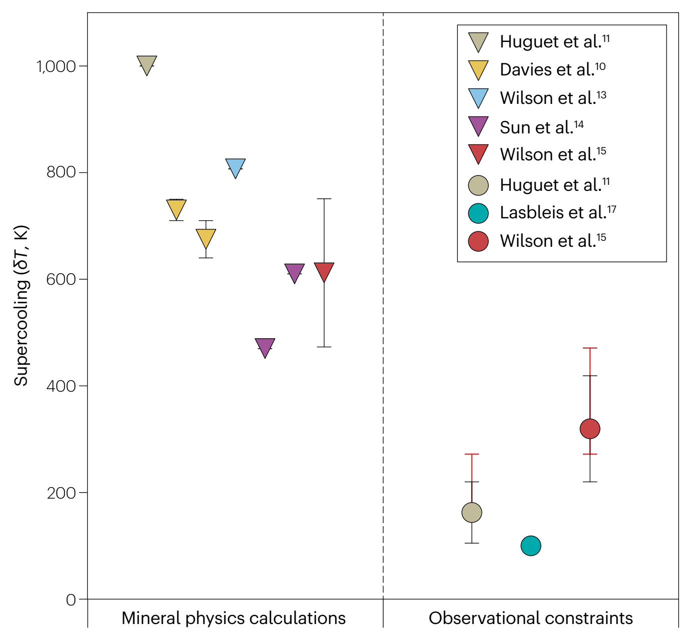

Fig. 2 | Estimates of supercooling in the Earth's core. The allowable supercooling for nucleation of the Earth's inner core inferred from geophysical observations (circles[11,15,17]; with a maximum of 419 K (ref. 15)) is compared to the estimated supercooling required to trigger nucleation of the inner core according to mineral physics calculations (triangles[10,11,13–15]; with a minimum of 467 K (ref. 15)). The black error bars relate to uncertainties associated with molecular dynamics calculations and inferences therein (left) and the uncertainty of core melting temperatures and adiabatic (right). The red uncertainty ranges show the effect of latent heat on estimates derived from inner core size. Multiple approaches have been used to identify a value of supercooling that is compatible with both the constraints set by geophysical observations and the physical requirements for nucleation defined by calculations, but none have been successful thus far.

boundary layer theory to determine the heat fluxes at the CMB (Q_{CMB}) and out of the convecting mantle, whereas the core model assumes the usual adiabatic, hydrostatic and chemically well-mixed state. The added complexities of a stably stratified layer[8,38], precipitation of oxides[9,31] below the CMB, the influence of a basal magma ocean at the base of the mantle[39,40], or alternative parameterizations of mantle dynamics[41,42] are not considered. Traditional thermal history models of the core define the inner core boundary at each time step as the intersection of the adiabat and the melting curve, which means that there is only one (equilibrium) growth regime and no supercooling. Here, we add the nucleation barrier and corresponding supercooling to these models by requiring that the centre of the core reaches a temperature lower than the melting temperature T_m by a prescribed supercooling value, δT, before the inner core nucleates (Fig. 1).

The key parameters determining core evolution are its chemical composition, temperature structure and thermal conductivity[2]. As in a previous work[5], three simple compositions are considered: $Fe_{0.82}O_{0.08}Si_{0.10}$, $Fe_{0.79}O_{0.13}Si_{0.08}$ and $Fe_{0.81}O_{0.17}Si_{0.02}$, which correspond to present-day inner core boundary density contrasts ($\delta\rho$) of 0.6 g cm^{-3}, 0.8 g cm^{-3} and 1.0 g cm^{-3}, respectively. These density contrasts match the range estimated from normal modes[43]. Increasing oxygen concentration increases the power supplied to the dynamo by compositional convection and decreases the melting point of the alloy. We explored a range of pure iron melting curves[44–46] and focus on the one[44] with the largest value at the centre of the Earth, which maximizes the available supercooling. For the supercooled region, we considered two temperature profiles: an adiabat matched to the temperature of the liquid core at the inner core boundary and an isothermal profile, wherein the entire supercooled region assumes the temperature at the inner core boundary (Supplementary Note 1). The isothermal profile is an extreme case that maximizes the actual supercooling that can be achieved and might arise owing to an increase in thermal conductivity with a depth that leads to stable stratification of the innermost core[47]. We consider three core thermal conductivity (k) values of 30, 50 and 70 W m^{-1} K^{-1} to explore low-conductivity, moderate-conductivity and moderately high-conductivity scenarios, respectively[5,48–50]. As we explain later in the Review, higher values of k proposed in earlier studies[47,48,51] would not increase the predicted δT and are, therefore, not considered. The supercooling is varied within the range inferred from geophysical observations (Fig. 2), which is compatible with the assumed core thermal structure. All other parameters remain unchanged from the original model[8].

For each parameter set, we tune the initial temperature of the core $T_{CMB}^{4.5\,Ga}$ and mantle $T_{mantle}^{4.5\,Ga}$ and the ratio of upper-to-lower mantle viscosity f_{visco} to satisfy four constraints: sufficient entropy available for ohmic dissipation such that the geodynamo has been active for the past 3.5 Gyr (refs. 52–56), the present inner core radius of 1,221 km, the current mid-mantle temperature of 2,320 ± 50 K (ref. 57), and the current heat loss of 38 ± 2 TW from the convective mantle[58]. We set $T_{mantle}^{4.5\,Ga}$ = 3,400 K for all cases where $\delta\rho$ = 0.6 or 0.8 g cm^{-3} and $T_{mantle}^{4.5\,Ga}$ = 3,000 K for $\delta\rho$ = 1.0 g cm^{-3}. We limit $T_{CMB}^{4.5\,Ga}$ to a maximum value of 7,000 K as extreme core temperatures imply a long-lived magma ocean. For consistency with prior implementations of this model[8,36,37], we only vary f_{visco} between 1 and 20.

Coupled core–mantle thermal histories for different k, $\delta\rho$ and δT with an adiabatic supercooled region produce a range of possible inner core ages and volumes of rapid initial freezing (Fig. 3; the isothermal case gives similar results, Supplementary Fig. 3). The case wherein δT = 0 K represents the traditional model of Driscoll and Davies[37]. All cases produce a young inner core less than 800 Myr old and a hot early CMB temperature >4,500 K, which exceeds current estimates of the lower mantle melting temperature[59], suggesting the existence of an early molten region above the core (Fig. 3a). The present-day CMB heat flux for solutions presented in Fig. 3 varies with composition and supercooling, with ranges of 9.2–9.9 TW, 9.1–9.2 TW and 8.2–8.4 TW for $\delta\rho$ = 0.6, 0.8 and 1.0 g cm^{-3}, respectively. These values are consistent with previous core thermal histories[2,5,6] despite the different model setups that have been used. The effect of changing core thermal conductivity is not particularly prominent in Fig. 3 because it only affects the power available to the dynamo and all values of k tested produce sufficient power at all times. The limiting factor for the success of these models within the parameter space explored, particularly $T_{CMB}^{4.5\,Ga}$ and f_{visco}, is matching the size of the inner core at the present day. The maximum supercooling that can be sustained before inner core nucleation in successful thermal histories is 77 K, although this case also requires the present-day T_{CMB} = 4,360 K that exceeds estimates of the mantle melting temperature[59], implying an extant basal magma ocean. Indeed, all cases where $\delta\rho$ = 0.6 g cm^{-3} fail in this regard. Cases where $\delta\rho$ = 0.8 and 1.0 g cm^{-3} have successful solutions with δT less than 60 K. Above this supercooling, all cases converge on an inner core age of 0 and a fast freezing region with radius 1,221 km because they require that the entire inner core froze in the immediate past. At modest supercooling (less than 30 K), the inner core age differs by up to ~400 Myr between cases. Models with larger $\delta\rho$ produce an older inner core because the enhanced gravitational energy release on freezing slows core cooling. Given the uncertainty in these models, we expect viable core thermal histories to require δT < 100 K.

A range of estimates exist for changes in seismic anisotropy with depth in the inner core (Fig. 3, grey histogram). Within this range, the radius of the innermost inner core has been estimated to be 300–750 km (refs. 60,61). To rapidly freeze this volume, the centre of the Earth must have been cooled by at least 5 K and by no more than 40 K, although this value depends on the composition of the core as $\delta\rho$ = 0.8 and 1.0 g cm^{-3} cases freeze 750-km-radius regions with δT ~35 K. Cases that are compatible with rapid freezing of an innermost inner core have inner core ages between 450 and 750 Myr.

Freezing of supercooled Fe liquids

We now return to consider the growth of the supercooled region. Growth rates observed in molecular dynamics simulations[13,15,34] suggest that the inner core could have frozen extremely rapidly, but these results do not consider the influence of latent heat release or the partitioning of light elements as the supercooled region freezes. Latent heat release could slow the growth rate if the heat is trapped in the supercooled region, thereby increasing the local temperature and decreasing the driving force ($\delta\mu$) for growth, which could occur if thermal conduction and core convection are too slow to transfer heat away from the freezing interface into the bulk core. We consider a simple model of this process that integrates equation (2) forward in time using a thermodynamic model based on the Fe–FeO system[62] to valuate $\delta\mu(P,T)$ and the calculated latent heat release to update an initially adiabatic temperature profile (Supplementary Note 6). When heat transfer is limited by thermal conduction, the results show that latent heat release slows the growth time of the supercooled region to ~100 years. This value is independent of the assumed initial size of the supercooled region because the limiting factor is the drop in g as the region grows towards the equilibrium point wherein the temperature of the supercooled region intersects the melting temperature. In reality,

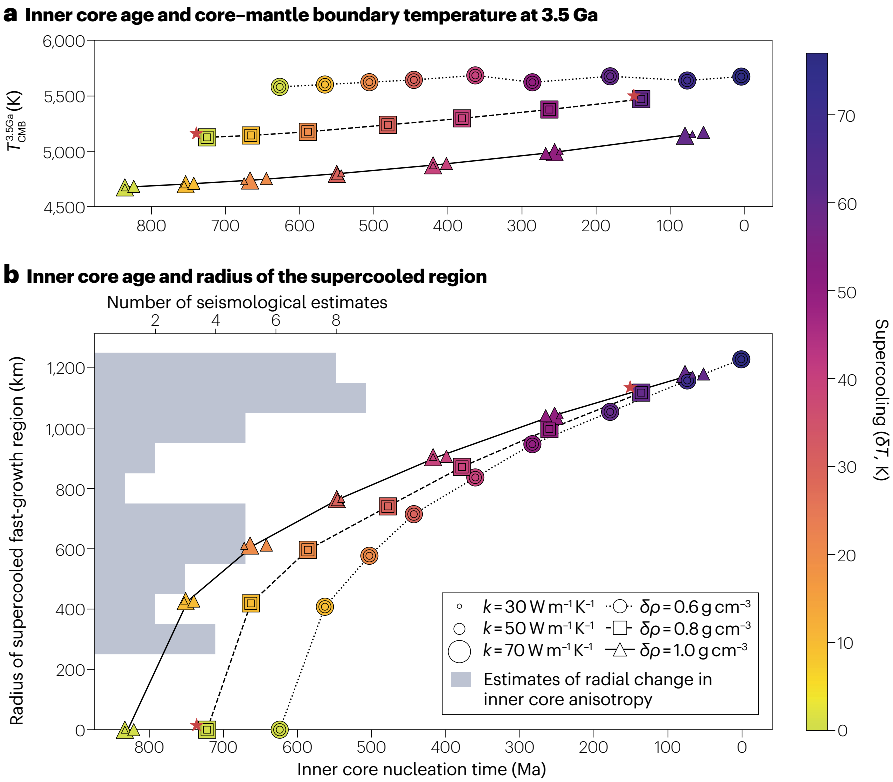

Fig. 3 | Supercooling impacts on core–mantle thermal histories. Thermal history model results of supercooling that match constraints on present-day inner core radius, mantle temperature and heat flux, as well as having sufficient entropy to drive the geodynamo for the past 3.5 Gyr. **a**, Variations in core–mantle boundary temperature at 3.5 Ga with inner core age. **b**, The inner core radius of the supercooled region before nucleation with inner core age. On both panels, symbols are coloured according to the imposed supercooling δT. Three compositions (circles, squares and triangles: $Fe_{0.82}O_{0.08}Si_{0.10}$, $Fe_{0.79}O_{0.13}Si_{0.08}$ and $Fe_{0.81}O_{0.17}Si_{0.02}$, respectively) and three thermal conductivities of the core (small, medium and large symbols: 30, 50 and 70 W m^{-1} K^{-1}) are explored. The supercooled region is assumed to be adiabatic (see Supplementary Note 4 for isothermal cases). Dipole moment is calculated for two thermal history cases (0 K and 60 K of supercooling before inner core nucleation, both with a thermal conductivity of 70 W m^{-1} K^{-1} and a density contrast at the inner core boundary of 0.8 g cm^{-3}) which are marked with red stars (and are shown on Fig. 6, where dipole moment is reported). The inset histogram (panel **b**, grey) shows the number of seismological estimates of radial changes in inner core anisotropy (Supplementary Note 5). Inner core age is more sensitive to supercooling of the core before inner core nucleation than it is to composition or thermal conductivity.

the latent heat would be expected to be removed by core convection. However, core convection occurs on a timescale of years, far slower than the rapid growth of the supercooled region. Nevertheless, the convective heat transport would only decrease the growth time from the ~100 years estimated here.

Light element partitioning offers another mechanism for slowing the freezing of supercooled liquids. Oxygen depresses the melting point of liquid iron, reducing δT for the same T_a, and is strongly partitioned to the liquid[22]. Light elements can only slow inner core growth by enriching a layer ahead of the growing inner core boundary and depressing the T_m of this layer. The removal of a light element-enriched liquid layer is controlled by diffusion and advection, making these processes the governors of inner core growth. If light elements are trapped in the growing inner core, chemical enrichment ahead of the inner core boundary is reduced. The liquid fraction of the inner core might be a result of dendritic inner core growth, but the rate and of liquid entrapment and volume of trapped liquid is poorly known[17]. Furthermore, the compaction of solids and rate at which light elements are lost from the trapped liquid through interstitial convection and diffusion are also not well understood. Nevertheless, once the inner core growth rate becomes comparable to the timescale of outer core overturn (hundreds of years), fluid advection will presumably become efficient at mixing the chemical anomaly into the bulk core. Therefore, the growth in the supercooled region is expected to be fast compared to the equilibrium growth phase.

The inner core is required to have had at least two growth phases: a rapid initial phase following supercooling of the liquid core and a slower in-equilibrium phase. The phase of rapid freezing might have concluded in O(100) years and can be comparable in size to the innermost inner core. Modelling of the subsequent slow growth phase is compatible with constraints on deep Earth evolution for a supercooling of <100 K and predicts that the inner core began to freeze less than 800 Ma.

Implications for inner core structure and dynamics

It is a physical requirement that the liquid core was supercooled before inner core nucleation. The exact amount of required supercooling remains enigmatic; however, $\delta T \leq 100$ K would be broadly consistent with inferences from geophysical observations (Figs. 2 and 3). In this section, we explore the consequences of supercooling for the structure and dynamics of the inner core through time and discuss how these implications might relate to seismic observations and the palaeomagnetic record.

Inner core structure

One of the key constraints on the thermal history of the deep Earth, the size of the inner core, comes from seismology[63]. The transition between solid and liquid iron at 1,221 km radius is assumed to define the intersection of T_m and T_a, fixing the present-day thermal state of the core. The inner core boundary is found to be sharp with a thickness of less than 3 km (ref. 64), although a laterally heterogeneous 4–8 km thick mushy layer between the inner and outer core might exist in some places[65]. The inner core grows primarily through direct freezing but could also grow as a result of an iron snow that forms in the lower outer core[66], although this mechanism has been suggested to be a minor contribution to growth[67]. If this iron snow regime is the relevant case, the thickness of the partially liquid region between the inner and outer core suggests that compaction of solids and expulsion of residual liquids upon late stages of core growth are efficient[17].

Seismic body waves and normal modes sampling the inner core reveal both radial and lateral heterogeneity (Fig. 4 and several review papers for a discussion[68,69]), but details of these features have been widely debated. Body waves are short period seismic data with a typical frequency of 0.1 to 1 Hz, which enables us to find small-scale structures, including layers and discontinuities. Normal modes are whole Earth oscillations with frequencies varying from 1 to 10 mHz and, therefore, are only sensitive to large-scale structures. Features seen with both body waves and normal modes are most robust, but it is also important to realize that some features could be challenging to observe with normal modes.

Body waves show that the outermost 60–100 km of the inner core consists of an isotropic layer where the eastern hemisphere transmits waves 1.5% faster than the western hemisphere[70,71]. This layer is also more strongly attenuating in the eastern hemisphere than in the western hemisphere[72]. Below this layer, the inner core is found to be anisotropic with seismic body waves travelling parallel to the rotational axis of the Earth, arriving several seconds earlier than those travelling parallel to the equatorial plane[73], and normal modes displaying anomalous zonal splitting[74]. Anisotropy is the most robust of all seismic features seen in the inner core because it is found in both body waves and normal modes. The rotational direction is 2–3.5%[75,76] and 3–5%[77–83] faster than average for normal mode and body wave seismicity, respectively. The anisotropy varies laterally wherein the western hemisphere appears to be more strongly anisotropic than the eastern hemisphere, which was initially only seen with body waves[84] but has also been confirmed by normal mode observations[85]. The orientation of the symmetry axis of inner core anisotropy might be varying regionally with the symmetry axis tilted towards the equatorial plane in the upper part of the inner core[85]. In the deeper part of the inner core (below ~710 km radius), the symmetry axis is found to be strongly aligned with the rotational axis of Earth[86]. Attenuation anisotropy might also exist wherein waves travelling in the direction of the rotation axis of Earth see more amplitude reduction than equatorially oriented waves[87,88]. Anisotropy also varies radially and increases with depth.

An innermost inner core has been proposed by several studies (for example, ref. 60). This innermost region represents a small sphere in the centre of the inner core with a radius of 300–750 km and has a distinct anisotropy with a different slowest direction compared to the outermost part of the inner core. The innermost inner core has been inferred by a range of different seismic data types, including body waves[60,89,90] and normal modestranm[91], but also multiple reflected

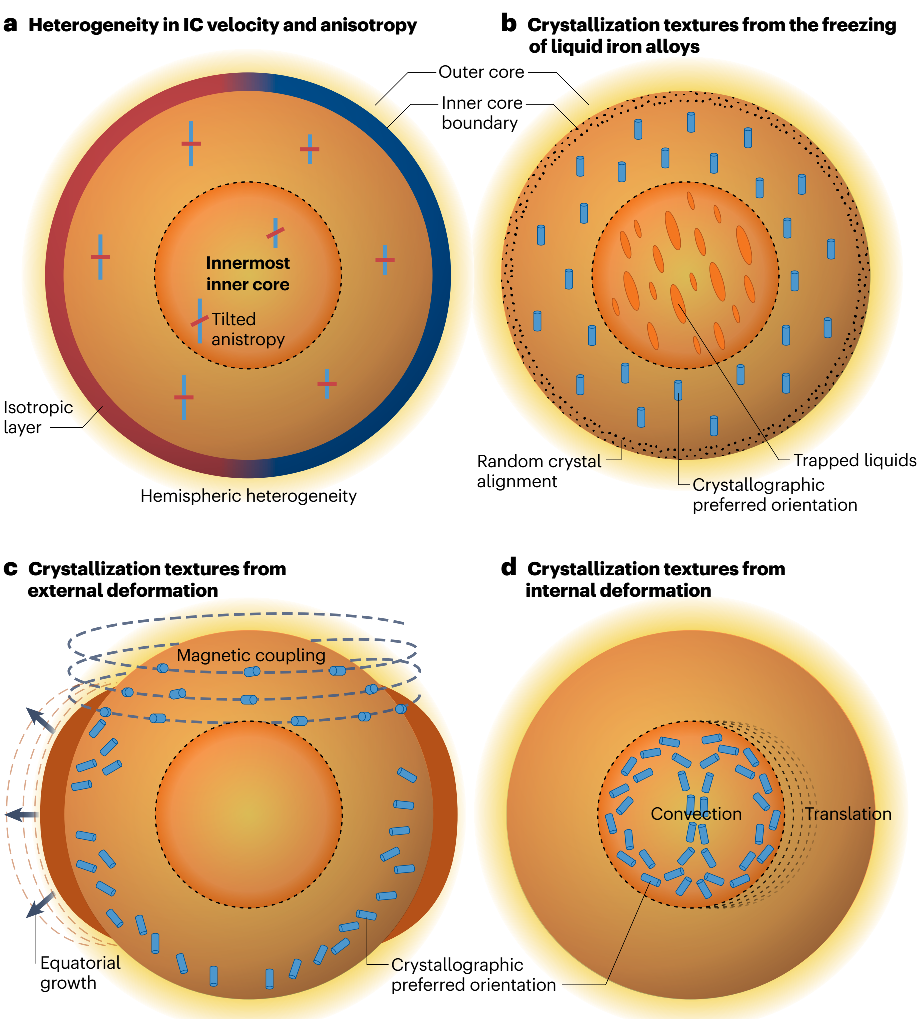

Fig. 4 | Observation and emplacement of inner core structure. a, Observed radial and lateral heterogeneity in the velocity (red and blue denoting relative slow and fast regions, respectively) and anisotropy of the Earth's inner core. These features result from compositional or textural heterogeneities that can have multiple origins, explored in panels **b**–**d**. **b**, Freezing of liquid iron alloys can produce different grain sizes and orientations and can trap liquids. **c**, External forces such as magnetic coupling and relaxation of heterogeneous equatorial growth can orient crystals in the inner core during or after their crystallization. **d**, Internal deformation mechanisms arising from inner core convection could establish stress regimes that reorient inner core crystals. The structure of the inner core inferred from seismology might have its origin in several mechanisms for developing texture, wherein rapid freezing textures, extensive trapped liquids and large-scale convection are unique to a supercooled core. IC, inner core.

waves[92], and it is also a very clear feature in inner core tomographic models[61,82].

The compilation of radial change in isotropic and anisotropic structure, both elastic and attenuating, at any depth in the inner core (refs. 60,61,70,71,79–84,90–117, Fig. 3) shows that there are two depths in which the anisotropy changes markedly. Near the top, around 1,100–1,200-km radius, the radial change signifies a switch from isotropic to anisotropic structure. Then, in a range of 300–750-km radius, there is the change to the innermost inner core structure.

Mechanisms to explain inner core texture

In this subsection, we focus primarily on the mechanisms that can explain the variations in elastic anisotropy with radius. We start with the traditional view that the core was never supercooled, then move on to mechanisms that involve supercooling.

Texturing in the absence of supercooling. Several mechanisms have been proposed that could generate the observed elastic anisotropy (Fig. 4). Solidification texturing aligns crystals during the freezing process[118,119], whereas deformation aligns the crystals after solidification and produces texture through accumulated strain. Several different deformation texturing mechanisms have been proposed. Internally induced deformation texturing can arise if the inner core is unstable to thermal or chemical convection[120]. Externally induced deformation texturing can arise via topographic relaxation of the inner core boundary driven by latitudinal variations in inner core growth associated with outer core convection[121], flow induced by coupling to the magnetic field[122,123], or flow driven by differential heat flux arising from outer core convection[90]. The dominant mechanism depends on the inner core growth history and material properties[124] and could have varied over time.

If the inner core is convectively unstable, then the strain produced by the resultant flow is expected to dominate over other deformation mechanisms[124]. The conditions for instability rely on some poorly known quantities, particularly the inner core growth rate and thermal and chemical diffusivities. Nevertheless, for plausible growth histories that ignore supercooling, there is a consensus that convection becomes less probable as the inner core grows and its growth rate declines[125–127]. For low values of the thermal conductivity (~30 W m^{-1} K^{-1}), an early episode of thermal convection is possible[126,128], whereas for the high conductivity values >100 W m^{-1} K^{-1} obtained by mineral physics calculations at inner core boundary conditions[51,129], it is very probable that thermal convection has never occurred. Compositional convection can be driven by a change in light element partitioning with depth[130] (and, hence, time); however, current models suggest that this destabilizing effect only dominates when the inner core is less than about half its present size[6]. Another possibility is that convection can result from imposed lateral heat flux variations at the inner core boundary[90], perhaps deriving from thermal interactions between the lower mantle and liquid core[131], although whether rapidly rotating convection can transmit such variations to the inner core boundary is currently debated[132].

In the early period, when the inner core was less than approximately half its present size and convection was possible, two distinct flow regimes have been identified that depend primarily on the inner core viscosity[124,128] η. For $\eta \lesssim 10^{18}$ Pa s, plume convection dominates and becomes increasingly chaotic as the Rayleigh number increases, whereas for higher η, a spherical harmonic degree 1 (hemispheric) translation emerges that can lead to melting of the inner core if the translation velocity is fast enough. A double diffusive form of the translation can arise even if the destabilizing compositional gradient is much weaker than the stabilizing thermal gradient, although this mode requires a higher viscosity and has a weaker velocity than pure thermal translation[133]. The resulting accumulated strain is probably weak for plume convection[134], because the flow is strongly time-dependent[124], and also the double diffusive translation, because the growth rate of the instability is on the order of inner core age[133] (100 Myr). For thermal translation, the strain rates can be appreciable as long as the viscosity is not too high. This flow is a good candidate for generating hemispheric asymmetry[135,136]. However, the strain field does not display the alignment with the rotation axis required to explain the cylindrical anisotropy.

For convectively stabilizing conditions, the primary strain-producing mechanisms are thought to be owing to topographic relaxation and magnetic coupling[124]. Topographic relaxation arises from the assumption (supported by numerical simulations[131]) that core convection enhances inner core boundary heat flow (and, hence, solidification rate) in the equatorial region, with isostatic adjustment driving a spherical harmonic degree 2 flow from the equatorial region towards the poles[121]. If the inner core is neutrally stratified, then the resulting flow penetrates deep into the inner core and can explain the general increase of anisotropy with depth[90,137]. However, with increasing stratification, the flow becomes confined to a thin layer below the inner core boundary with negligible deformation at depth[125,137] unless the viscosity is very high (~10^{23} Pa s (ref. 124)), in which case the strain rates decline substantially. The flow induced through coupling to the azimuthal component of the Lorentz force is unaffected by stratification[138] and yields an accumulated strain that is maximum at mid-depth[139]. However, the mechanism relies on a low viscosity of $\eta \lesssim 10^{12}$ Pa s in order for the strain rate to exceed that from topographic relaxation of equatorial growth. The mechanism also relies on an assumed configuration of the magnetic field at the inner core boundary now and back in time, which is not directly observable.

In summary, in the absence of supercooling, the inner core appears to have been stably stratified throughout most of its history, suggesting that convection is not the primary cause of radial anisotropy variations. The most probable deformation texturing mechanisms are magnetic coupling through the azimuthal Lorentz force, which requires a low viscosity, or topographic coupling, which requires a high viscosity and a timescale for texture development on the order of the inner core age. Hemispherical growth could also produce the outer isotropic layer if the stratification is strong enough[125]. These mechanisms could be augmented by other processes such as translational flow induced by lateral heat flow variations at the inner core boundary, which might be important for explaining the hemispheric asymmetry.

Texturing resulting from supercooling. We now discuss how the dynamic mechanisms that can explain inner core structure change with the addition of supercooling. The key difference is the period of rapid growth following nucleation, which alters the dynamical processes that can cause deformation in the deep inner core.

Following nucleation, the inner core growth rate is estimated to be far in excess of ~1 mm yr^{-1} (see discussion in the 'Inner core cooling and growth' section). This growth rate yields a Rayleigh number that far exceeds the critical value for instability for any value of the viscosity[128]. The critical values published to date[128] have ignored the time dependence of the basic diffusive state, which could be important in the rapid growth regime. Nevertheless, the available values indicate that the inner core was initially inevitably unstable to both plume and translation modes of convection. However, the supercooled region would have frozen in perhaps only a century, and after diffusive transport removed latent heat from the inner core, the Rayleigh number probably fell below the critical value for convection, which means that convection might not have persisted for more than several overturns. A detailed study of the flow instability in this scenario would require modelling the coupled dynamics of inner and outer core because the two systems evolve on similar timescales. However, present estimates of the growth rate for both plume and translation flows, which again neglect the rapid change of the basic state, are estimated to be a few tens of millions of years[128], suggesting that the instability would not develop despite the strongly unstable conditions. Whereas this situation does not exclude a brief episode of convection, prolonged overturning appears not probable.

Texturing of the supercooled material could arise either from solidification texturing, magnetic coupling (penetrating the rapidly frozen region), or equatorial growth. Magnetic coupling during fast freezing might be relatively unaffected by rapid cooling if the abrupt changes in geometry and thermo-chemical buoyancy have a relatively short-term (on the order of 100 years) impact on the dynamo. For equatorial growth, a key factor is the length of time required to establish the stratified thermal and chemical profiles from the temperature and composition at which the material froze (presumably between the adiabatic well-mixed pre-nucleation state and the liquidus). If this timescale is short, then the initial flow induced by topographic relaxation would be confined to the edge of the supercooled region; otherwise, the flow can penetrate to the centre of the core.

Rapid crystal growth might trap liquids within the inner core. The shape of liquid inclusions and mineralogy resulting from their eventual freezing could influence the attenuation and velocity anisotropy of this region. Partitioning of light elements to the liquid can depress the melting temperature of these trapped liquids, delaying freezing. The degree to which this effect is preserved to the present day depends strongly on the compaction efficiency of the newly formed crystal matrix[17,121] and partitioning behaviour during quenching, neither of which are well understood at core conditions. Owing to light element partitioning, these inclusions might freeze slowly as the inner core cooled and 3–10%[18] of the inner core could remain liquid at the present day, providing a plausible explanation for anomalously slow S-wave speeds[140] in the bulk inner core when compared to mineral physics[141,142]. The slower freezing rate of trapped liquids could imprint a heterogeneous texture in the innermost inner core and explain why its anisotropy is different compared to the shallower parts of the inner core[17]. One mechanism for this structure is for the crystals freezing in these liquid inclusions to experience magnetic coupling. Ab initio calculations[143,144] have shown that the principal axis of magnetic susceptibility in hexagonally close packed Fe is orthogonal to the axis of elastic anisotropy. If magnetically coupled, crystals would have an elastic anisotropic alignment parallel to the rotation axis of the core. The field strength needed to align the crystal structure in the solid is probably very strong[144], but if crystals grow within liquid inclusions, exposed to the magnetic field but isolated from convection, texturing is more plausible. Similarly, crystal growth within liquid inclusions could be enhanced along principal heat flux directions[119] producing a textural alignment flowing from the equator to the poles[121].

The introduction of supercooling opens the possibility that a rapidly frozen region accounts for some or all of the radial heterogeneity in the inner core (Fig. 5). Inner core translation is the current best candidate to explain lateral heterogeneity, but supercooling might help with initiation of offset inner core growth. Because nucleation can occur anywhere with the supercooled volume, fast freezing could begin away from the centre of the Earth, and this offset might initiate translational growth or offset texturing. Convection in the supercooled region might have been short lived despite the strongly unstable conditions because the timescale for instability, defined by the diffusion of latent heat out of the inner core, is probably two or more orders of magnitude longer than the rapid freezing timescale. The viability of texture development by magnetic coupling or heterogeneous growth is less clear than in the traditional case with no supercooling because it depends on the uncertain properties of the growth process. Solidification textures resulting from rapid freezing of the supercooled region and liquid inclusions captured in the process tend to be distinct from those associated with slower growth. A more detailed model of freezing and partitioning under supercooled conditions at high temperature and pressure is required to understand the potential for generating anisotropic texture in the inner core. Additionally, an improved understanding of geodynamo activity during and following a rapid freezing event is needed to qualify magnetic coupling.

Palaeomagnetic evidence of inner core growth

The palaeomagnetic record captures long-term changes in the strength of the magnetic field. Nucleation of the inner core might have an observable signature in the record in a number of ways. Theoretical models without supercooling[6,145,146] suggest that over time, the dynamo power and, hence, the dipole moment declines to a weak state directly preceding inner core formation; after which, latent heat and gravitational energy release from inner core growth provide substantial excess power to the geodynamo, causing a sudden increase in field strength (Fig. 6). An ultra-low dipole moment followed by a rapid increase has been reported in the early Cambrian[147–150], and weak fields have also been reported in the neo-proterozoic[151], although some high intensities around 1.1 Ga appear inconsistent with the simple theoretical prediction[152]. The addition of supercooling changes the theoretical prediction in two ways. First, increasing δT decreases the theoretical inner core age (Fig. 3) and increases the predicted rate of dipole moment intensification at the formation of the inner core (Fig. 6). This information will hopefully enable future palaeomagnetic analyses to constrain the minimum age of the inner core that is compatible with the palaeointensity record, which should improve existing bounds on the viable supercooling (Fig. 2). Second, rapid growth of the supercooled region and the associated release of latent heat and gravitational energy from chemical partitioning (which is not included in the models in Fig. 6) should drastically increase the power available to the dynamo, which could have left an imprint on the palaeomagnetic record[11]. Power-based scaling laws[145,146] derived from simulations of the dynamo in the past 100 Myr would predict a dramatic increase in the surface dipole field strength during this period, which could far exceed that shown by the purple line in Fig. 6. However, simulations also show that increased thermo-chemical driving eventually leads to a loss of axial dipole dominance and a weak multipolar field[153,154]. Therefore, the rapid increase in field strength could be curtailed by dipole collapse, followed by a period of weak highly variable field behaviour. Future dynamo simulations and palaeomagnetic analyses will hopefully shed more light on this issue.

Supercooling of the Earth's core before inner core nucleation is expected to have both seismological and palaeomagnetic signatures. Inner core features defined by anisotropy and attenuation, for

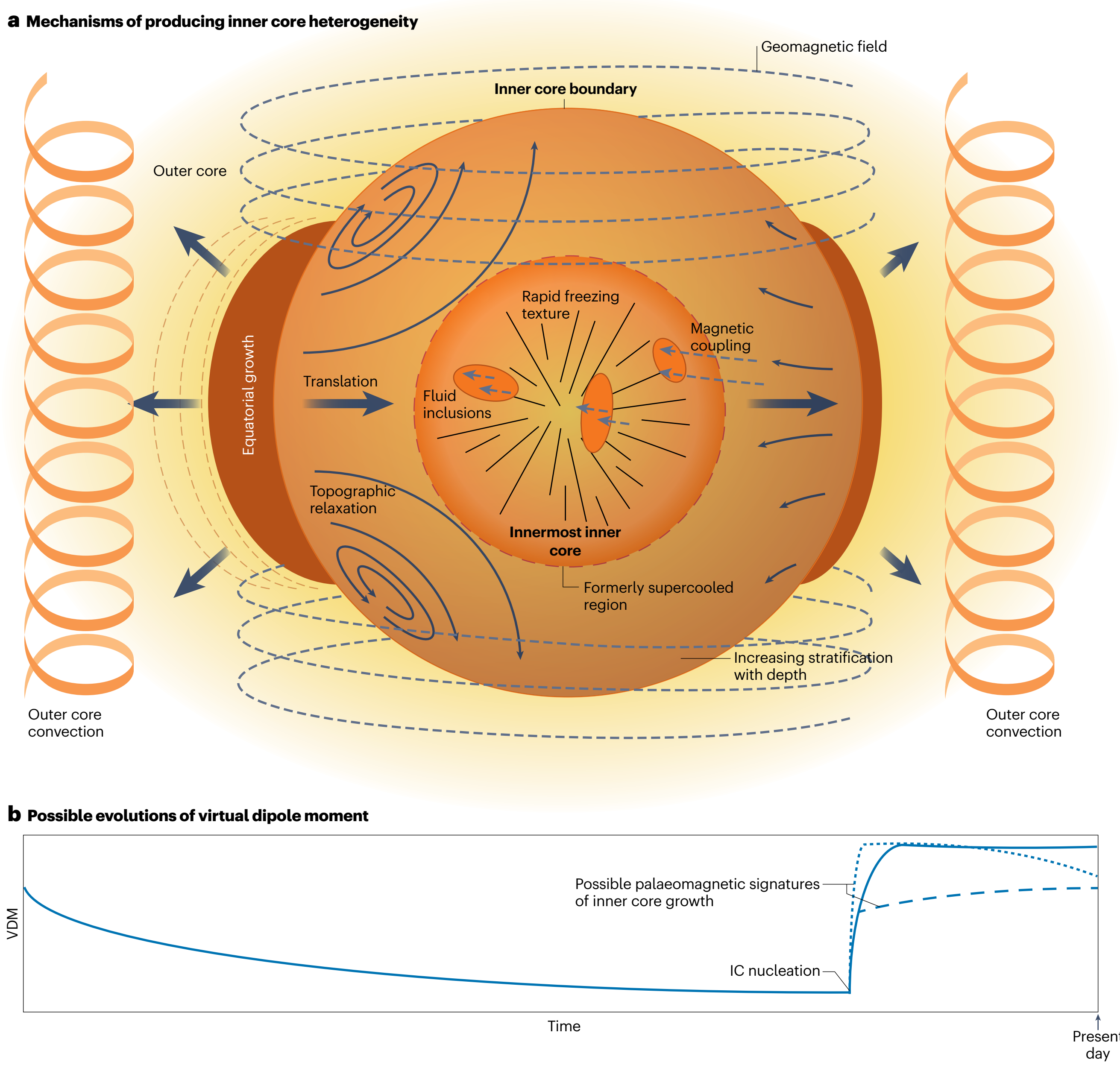

Fig. 5 | Multiple mechanisms exist for producing inner core heterogeneity. **a**, Without supercooling, equatorial growth, thermal and chemical convection, translational growth and magnetic coupling all offer routes to generate heterogeneous textures in the inner core. With supercooling, some of these textures are modified or apply to different regions of the inner core; for example, rapid growth of the inner core introduces the potential for unique texturing from solidification and trapped liquids. **b**, The virtual dipole moment (VDM) produced by different supercooling, and therefore thermal, histories. The VDM might vary greatly and is testable using the palaeomagnetic rock record. Multiple mechanisms for developing texture in the inner core might be needed to explain all seismologically detected structures. IC, inner core.

example, the innermost inner core, could be explained by texturing from rapid inner core growth or the associated convection. Rapid increases in palaeomagnetic intensity or dipole collapse could be attributed to the sudden release of latent heat and light elements associated with rapid inner core growth. The identification of these signatures requires new texturing and geodynamo models that incorporate a supercooled core.

Summary and future perspectives

Supercooling is required to initiate freezing of the Earth's solid inner core, as with any liquid. The degree to which the liquid core was supercooled before nucleation remains enigmatic but is crucial for understanding the deep interior of Earth. Molecular dynamics simulations of liquid iron alloys at the conditions of Earth's core suggest that >450 K of supercooling is required for spontaneous freezing. However,

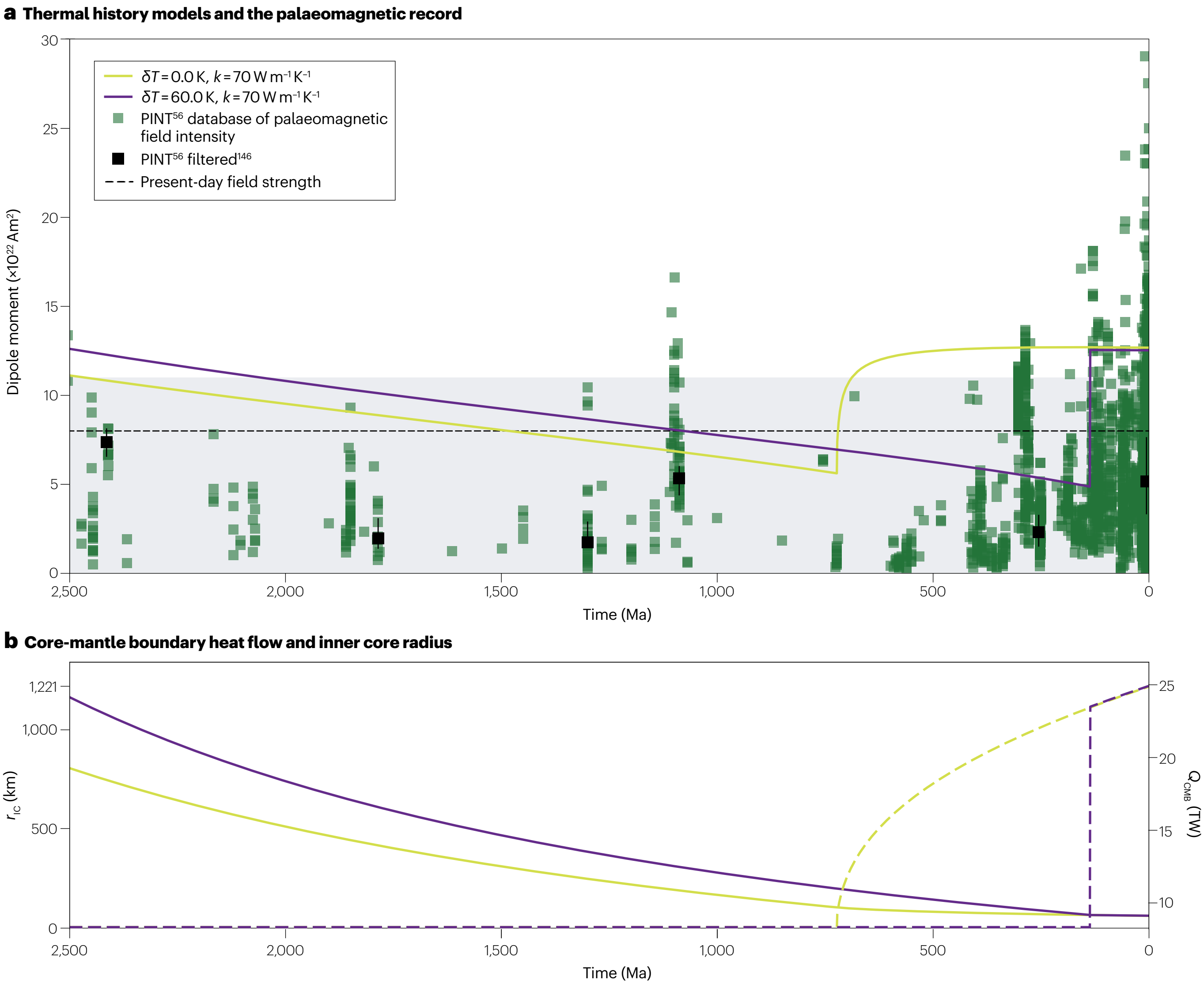

Fig. 6 | Comparing thermal history models with the palaeomagnetic record. a, Curves represent dipole moments calculated from two thermal history cases (red stars, Fig. 3), both with (purple curve) and without (yellow curve) supercooling before nucleation. Dipole moment calculated from palaeomagnetic intensity data (green squares: PINT[56]; black squares: filtered PINT dataset[146]) and the present-day field strength (black dashed line[146]) are shown for comparison. **b**, CMB heat flow (solid curves) is shown for the same cases as in panel **a**, alongside the inner core radius with time (dashed curves). Thermal history models with supercooling greater than 40 K produce a core less than 300 Myr old, which is challenging to reconcile with the palaeomagnetic record that shows consistently high field strength during this period.

geophysical constraints are only compatible with supercooling less than 420 K, but more probably less than 100 K.

To complete the picture of inner core nucleation, a viable resolution to the inner core nucleation paradox is needed. Solving the paradox will reveal an acceptable value of supercooling in the core and enable the development of thermal history models that are consistent with both mineral physics and observations. The simple binary compositions tested in previous studies have fallen short of identifying a definitive resolution from homogeneous nucleation. A resolution to the inner core nucleation paradox requires new mineral physics calculations that explore ternary compositions in the core. Heterogeneous nucleation should be explored, although at the time of writing, the cores of impacting planetesimals, gold and copper, tungsten carbide and several oxides have been ruled out as heterogeneous nucleation sites in the core. Research into dense solid phases that avoid dissolution and melting in the core is needed to identify a resolution to the paradox via heterogeneous nucleation.

Calculations of alloy freezing rates suggest that inner core growth following the nucleation event was extremely fast, but crystal growth behaviour under core conditions at these rates is poorly understood. Both experimental and computational research is needed to better understand freezing textures, element partitioning and residual liquid entrapment at scales ranging from angstroms to metres. This will improve predictions of inner core growth and reveal the textural, structural and thermo-chemical fingerprints of inner core nucleation that might be identified through palaeomagnetic and seismological investigation. These advances are essential for understanding how inner core nucleation has impacted the dynamics of the inner core, especially with regard to convective instabilities in the growing inner core and the potential for associated palaeomagnetic expressions. The present view of outer core dynamics typically assumes that inner core growth occurs on a timescale of at least 100,000 years, at least two orders of magnitude slower than inner core growth from supercooled liquids. New dynamo calculations and scaling laws are needed to describe outer core dynamics when the inner and outer cores evolve on comparable timescales, as could be the case during the rapid growth phase of the inner core.

Finally, a model that explains all seismically inferred inner core structure does not yet exist. This Review has highlighted that of the existing mechanisms to develop crystallographic texture in the solid inner core, some are unique to a supercooled liquid core, some are modified by this supercooled scenario and other mechanisms are independent of supercooling. The thermal history models discussed here might explain two seismically distinct regions of the inner core resulting from rapid freezing and subsequent slower growth but do not explain lateral heterogeneity or the presence of more than two layers. Any of the proposed mechanisms that can texture the inner core are confined to specific regions (for example, the outermost region has the highest tendency to be textured by topographic relaxation) and are capable of overprinting prior texturing. Therefore, matching mechanisms to seismological data is complex. To address this issue, a holistic thermal history model of the inner core that describes freezing, dynamics and crystallographic deformation within a coherent framework is needed.

Data availability

The data for the inset histogram of seismological estimates of inner core structure in Fig. 3 can be found in Supplementary Table 1.

Published online: 12 February 2025

References

1. Birch, F. The melting relations of iron, and temperatures in the Earth's core. *Geophys. J. R. Astron. Soc.* **29**, 373–387 (1972).
2. Nimmo, F. Thermal and compositional evolution of the core. *Treatise Geophys.* **9**, 201–219 (2015).
3. Braginsky, S. I. Structure of the F layer and reasons for convection in the Earth's core. *Sov. Phys. Dokl*. **149**, 8–10 (1963).
4. Stevenson, D. J. Mars' core and magnetism. *Nature* **412**, 214–219 (2001).
5. Davies, C., Pozzo, M., Gubbins, D. & Alfè, D. Constraints from material properties on the dynamics and evolution of Earth's core. *Nat. Geosci.* **8**, 678–685 (2015).
6. Labrosse, S. Thermal evolution of the core with a high thermal conductivity. *Phys. Earth Planet. Inter.* **247**, 36–55 (2015).
7. Davies, C. Cooling history of Earth's core with high thermal conductivity. *Phys. Earth Planet. Inter.* **247**, 65–79 (2015).
8. Greenwood, S., Davies, C. J. & Mound, J. E. On the evolution of thermally stratified layers at the top of Earth's core. *Phys. Earth Planet. Inter.* **318**, 106763 (2021).
9. Wilson, A. J. et al. Powering Earth's ancient dynamo with silicon precipitation. *Geophys. Res. Lett.* **49**, e2022GL100692 (2022).
10. Davies, C., Pozzo, M. & Alfè, D. Assessing the inner core nucleation paradox with atomic-scale simulations. *Earth Planet. Sci. Lett.* **507**, 1–9 (2019).
11. Huguet, L., Van Orman, J. A., Hauck, S. A. II & Willard, M. A. Earth's inner core nucleation paradox. *Earth Planet. Sci. Lett.* **487**, 9–20 (2018).
12. Christian, J. W. *The Theory of Transformations in Metals and Alloys* (Newnes, 2002).
13. Wilson, A. J., Walker, A. M., Alfè, D. & Davies, C. J. Probing the nucleation of iron in Earth's core using molecular dynamics simulations of supercooled liquids. *Phys. Rev. B* **103**, 214113 (2021).
14. Sun, Y., Zhang, F., Mendelev, M. I., Wentzcovitch, R. M. & Ho, K.-M. Two-step nucleation of the Earth's inner core. *Proc. Natl Acad. Sci. USA* **119**, e2113059119 (2022).
15. Wilson, A. J., Alfè, D., Walker, A. M. & Davies, C. J. Can homogeneous nucleation resolve the inner core nucleation paradox? *Earth Planet. Sci. Lett.* **614**, 118176 (2023).
16. Tarduno, J. A. et al. Geodynamo, solar wind, and magnetopause 3.4 to 3.45 billion years ago. *Science* **327**, 1238–1240 (2010).
17. Lasbleis, M., Kervazo, M. & Choblet, G. The fate of liquids trapped during the Earth's inner core growth. *Geophys. Res. Lett.* **47**, e2019GL085654 (2020).
18. Singh, S. C., Taylor, M. A. J. & Montagner, J. P. On the presence of liquid in Earth's inner core. *Science* **287**, 2471–2474 (2000).
19. Pang, G. et al. Enhanced inner core fine-scale heterogeneity towards Earth's centre. *Nature* **620**, 570–575 (2023).
20. Alfè, D., Gillan, M. J. & Price, G. D. Composition and temperature of the Earth's core constrained by combining ab initio calculations and seismic data. *Earth Planet. Sci. Lett.* **195**, 91–98 (2002).
21. Li, Y., Vočadlo, L., Alfè, D. & Brodholt, J. Carbon partitioning between the Earth's inner and outer core. *J. Geophys. Res. Solid Earth* **124**, 12812–12824 (2019).
22. Alfè, D., Gillan, M. J. & Price, G. D. Temperature and composition of the Earth's core. *Contemp. Phys.* **48**, 63–80 (2007).
23. Wood, B. J., Li, J. & Shahar, A. Carbon in the core: its influence on the properties of core and mantle. *Rev. Miner. Geochem.* **75**, 231–250 (2013).
24. Blanchard, I. et al. The metal-silicate partitioning of carbon during Earth's accretion and its distribution in the early solar system. *Earth Planet. Sci. Lett.* **580**, 117374 (2022).
25. Smith, E. M. et al. Large gem diamonds from metallic liquid in Earth's deep mantle. *Science* **354**, 1403–1405 (2016).
26. Badro, J. et al. Magnesium partitioning between Earth's mantle and core and its potential to drive an early exsolution geodynamo. *Geophys. Res. Lett.* **45**, 13–240 (2018).
27. Fischer, R. A., Campbell, A. J. & Ciesla, F. J. Sensitivities of Earth's core and mantle compositions to accretion and differentiation processes. *Earth Planet. Sci. Lett.* **458**, 252–262 (2017).
28. Hirose, K. et al. Crystallization of silicon dioxide and compositional evolution of the Earth's core. *Nature* **543**, 99–102 (2017).
29. Wilson, A. J., Pozzo, M., Davies, C. J., Walker, A. M. & Alfè, D. Examining the power supplied to Earth's dynamo by magnesium precipitation and radiogenic heat production. *Phys. Earth Planet. Inter.* **343**, 107073 (2023).
30. O'Rourke, J. G. & Stevenson, D. J. Powering Earth's dynamo with magnesium precipitation from the core. *Nature* **529**, 387–389 (2016).
31. Badro, J., Siebert, J. & Nimmo, F. An early geodynamo driven by exsolution of mantle components from Earth's core. *Nature* **536**, 326–328 (2016).
32. Eustathopoulos, N. Wetting by liquid metals — application in materials processing: the contribution of the Grenoble group. *Metals* **5**, 350–370 (2015).
33. Spaepen, F. & Turnbull, D. in *Rapidly Quenched Metals* (eds Grant, N. J. & Giessen, B. C.) 205 (MIT Press, 1976).
34. Sun, G., Xu, J. & Harrowell, P. The mechanism of the ultrafast crystal growth of pure metals from their melts. *Nat. Mater.* **17**, 881–886 (2018).
35. Coriell, S. R. & Turnbull, D. Relative roles of heat transport and interface rearrangement rates in the rapid growth of crystals in undercooled melts. *Acta Metall.* **30**, 2135–2139 (1982).
36. Driscoll, P. & Bercovici, D. On the thermal and magnetic histories of Earth and Venus: influences of melting, radioactivity, and conductivity. *Phys. Earth Planet. Inter.* **236**, 36–51 (2014).
37. Driscoll, P. & Davies, C. The "New Core Paradox": challenges and potential solutions. *J. Geophys. Res. Solid Earth* **128**, e2022JB025355 (2023).
38. Buffett, B. A. & Seagle, C. T. Stratification of the top of the core due to chemical interactions with the mantle. *J. Geophys. Res. Solid Earth* **115**, B04407 (2010).
39. Labrosse, S., Hernlund, J. W. & Coltice, N. A crystallizing dense magma ocean at the base of the Earth's mantle. *Nature* **450**, 866–869 (2007).
40. Davies, C. J. & Greenwood, S. in *Core-Mantle Co-Evolution: An Interdisciplinary Approach* (eds Nakagawa, T. et al.) Ch. 12 (American Geophysical Union, 2023).
41. O'Rourke, J. G., Korenaga, J. & Stevenson, D. J. Thermal evolution of Earth with magnesium precipitation in the core. *Earth Planet. Sci. Lett.* **458**, 263–272 (2017).
42. Al Asad, M., Lau, H. C. P., Crowley, J. W. & Lenardic, A. Modes of mantle convection, their stability, and what controls their existence. *J. Geophys. Res. Solid Earth* **128**, e2023JB027274 (2023).
43. Masters, G. & Gubbins, D. On the resolution of density within the Earth. *Phys. Earth Planet. Inter.* **140**, 159–167 (2003).
44. Alfè, D., Price, G. D. & Gillan, M. J. Iron under Earth's core conditions: liquid-state thermodynamics and high-pressure melting curve from ab initio calculations. *Phys. Rev. B* **65**, 165118 (2002).
45. Sinmyo, R., Hirose, K. & Ohishi, Y. Melting curve of iron to 290 GPa determined in a resistance-heated diamond-anvil cell. *Earth Planet. Sci. Lett.* **510**, 45–52 (2019).
46. Li, J. et al. Shock melting curve of iron: a consensus on the temperature at the Earth's inner core boundary. *Geophys. Res. Lett.* **47**, e2020GL087758 (2020).
47. Gomi, H. et al. The high conductivity of iron and thermal evolution of the Earth's core. *Phys. Earth Planet. Inter.* **224**, 88–103 (2013).
48. Pozzo, M., Davies, C., Gubbins, D. & Alfè, D. Thermal and electrical conductivity of iron at Earth's core conditions. *Nature* **485**, 355–358 (2012).
49. Konôpková, Z., McWilliams, R. S., Gomez-Perez, N. & Goncharov, A. F. Direct measurement of thermal conductivity in solid iron at planetary core conditions. *Nature* **534**, 99–101 (2016).
50. Zhang, Y. et al. Reconciliation of experiments and theory on transport properties of iron and the geodynamo. *Phys. Rev. Lett.* **125**, 78501 (2020).

51. Pozzo, M., Davies, C., Gubbins, D. & Alfè, D. Thermal and electrical conductivity of solid iron and iron-silicon mixtures at Earth's core conditions. *Earth Planet. Sci. Lett.* **393**, 159–164 (2014).
52. Biggin, A. J. et al. Palaeomagnetic field intensity variations suggest Mesoproterozoic inner-core nucleation. *Nature* **526**, 245–248 (2015).
53. Tarduno, J. A., Cottrell, R. D., Davis, W. J., Nimmo, F. & Bono, R. K. A Hadean to Paleoarchean geodynamo recorded by single zircon crystals. *Science* **349**, 521–524 (2015).
54. Tarduno, J. A. et al. Paleomagnetism indicates that primary magnetite in zircon records a strong Hadean geodynamo. *Proc. Natl Acad. Sci. USA* **117**, 2309–2318 (2020).
55. Fu, R. R. et al. Paleomagnetism of 3.5-4.0 Ga zircons from the Barberton Greenstone Belt, South Africa. *Earth Planet. Sci. Lett.* **567**, 116999 (2021).
56. Bono, R. K. et al. The PINT database: a definitive compilation of absolute palaeomagnetic intensity determinations since 4 billion years ago. *Geophys. J. Int.* **229**, 522–545 (2022).
57. Katsura, T., Yoneda, A., Yamazaki, D., Yoshino, T. & Ito, E. Adiabatic temperature profile in the mantle. *Phys. Earth Planet. Inter.* **183**, 212–218 (2010).
58. Jaupart, C., Labrosse, S., Lucazeau, F. & Mareschal, J. C. Temperatures, heat and energy in the mantle of the earth. *Treatise Geophys.* **7**, 223–270 (2007).
59. Andrault, D. et al. Solidus and liquidus profiles of chondritic mantle: implication for melting of the Earth across its history. *Earth Planet. Sci. Lett.* **304**, 251–259 (2011).
60. Ishii, M. & Dziewoński, A. M. The innermost inner core of the earth: evidence for a change in anisotropic behavior at the radius of about 300 km. *Proc. Natl Acad. Sci. USA* **99**, 14026–14030 (2002).
61. Brett, H., Hawkins, R., Waszek, L., Lythgoe, K. & Deuss, A. 3D transdimensional seismic tomography of the inner core. *Earth Planet. Sci. Lett.* **593**, 117688 (2022).
62. Komabayashi, T. Thermodynamics of the system Fe-Si-O under high pressure and temperature and its implications for Earth's core. *Phys. Chem. Min.* **47**, 1–13 (2020).
63. Dziewonski, A. M. & Anderson, D. L. Preliminary reference Earth model. *Phys. Earth Planet. Inter.* **25**, 297–356 (1981).
64. Koper, K. D., Pyle, M. L. & Franks, J. M. Constraints on aspherical core structure from PKiKP-PcP differential travel times. *J. Geophys. Res. Solid Earth* https://doi.org/10.1029/2002JB001995 (2003).
65. Tian, D. & Wen, L. Seismological evidence for a localized mushy zone at the Earth's inner core boundary. *Nat. Commun.* **8**, 165 (2017).
66. Wong, J., Davies, C. J. & Jones, C. A. A regime diagram for the slurry F-layer at the base of Earth's outer core. *Earth Planet. Sci. Lett.* **560**, 116791 (2021).
67. Wilczyński, F., Davies, C. J. & Jones, C. A. A two-phase pure slurry model for planetary cores: one-dimensional solutions and implications for Earth's F-layer. *J. Fluid Mech.* **976**, A5 (2023).
68. Deuss, A. Heterogeneity and anisotropy of Earth's inner core. *Annu. Rev. Earth Planet. Sci.* **42**, 103–126 (2014).
69. Tkalcic, H. *The Earth's Inner Core Revealed by Observational Seismology* (Cambridge Univ. Press, 2017).
70. Niu, F. & Wen, L. Hemispherical variations in seismic velocity at the top of the Earth's inner core. *Nature* **410**, 1081–1084 (2001).
71. Waszek, L. & Deuss, A. Distinct layering in the hemispherical seismic velocity structure of Earth's upper inner core. *J. Geophys. Res. Solid Earth* **116**, B12313 (2011).
72. Yu, W. & Wen, L. Seismic velocity and attenuation structures in the top 400 km of the Earth's inner core along equatorial paths. *J. Geophys. Res.* **112**, B07308 (2006).
73. Morelli, A., Dziewonski, A. M. & Woodhouse, J. H. Anisotropy of the inner core inferred from PKIKP travel times. *Geophys. Res. Lett.* **13**, 1545–1548 (1986).
74. Woodhouse, J. H., Giardini, D. & Li, X. D. Evidence for inner core anisotropy from free oscillations. *Geophys. Res. Lett.* **13**, 1549–1552 (1986).
75. Tromp, J. Support for anisotropy of the Earth's inner core from free oscillations. *Nature* **366**, 678–681 (1993).
76. Deuss, A., Ritsema, J. & van Heijst, H. A new catalogue of normal-mode splitting function measurements up to 10 mHz. *Geophys. J. Int.* **193**, 920–937 (2013).
77. Creager, K. C. Anisotropy of the inner core from differential travel times of the phases PKP and PKIKP. *Nature* **356**, 309–314 (1992).
78. Vinnik, L., Romanowicz, B. & Breger, L. Anisotropy in the center of the inner core. *Geophys. Res. Lett.* **21**, 1671–1674 (1994).
79. McSweeney, T. J., Creager, K. C. & Merrill, R. T. Depth extent of inner-core seismic anisotropy and implications for geomagnetism. *Phys. Earth Planet. Inter.* **101**, 131–156 (1997).
80. Creager, K. C. Large-scale variations in inner core anisotropy. *J. Geophys. Res. Solid Earth* **104**, 23127–23139 (1999).
81. Garcia, R. & Souriau, A. Inner core anisotropy and heterogeneity level. *Geophys. Res. Lett.* **27**, 3121–3124 (2000).
82. Sun, X. & Song, X. Tomographic inversion for three-dimensional anisotropy of Earth's inner core. *Phys. Earth Planet. Inter.* **167**, 53–70 (2008).
83. Irving, J. C. E. & Deuss, A. Hemispherical structure in inner core velocity anisotropy. *J. Geophys. Res. Solid Earth* https://doi.org/10.1029/2010JB007942 (2011).
84. Tanaka, S. & Hamaguchi, H. Degree one heterogeneity and hemispherical variation of anisotropy in the inner core from PKP (BC)-PKP (DF) times. *J. Geophys. Res. Solid Earth* **102**, 2925–2938 (1997).
85. Deuss, A., Irving, J. C. E. & Woodhouse, J. H. Regional variation of inner core anisotropy from seismic normal mode observations. *Science* **328**, 1018–1020 (2010).
86. Brett, H., Tromp, J. & Deuss, A. Tilted transverse isotropy in Earth's inner core. *Nat. Geosci.* **17**, 1059–1064 (2024).
87. Souriau, A. & Romanowicz, B. Anisotropy in inner core attenuation: a new type of data to constrain the nature of the solid core. *Geophys. Res. Lett.* **23**, 1–4 (1996).
88. Makinen, A. M. & Deuss, A. Normal mode splitting due to inner core attenuation anisotropy. *Geophys. J. Int.* **195**, 1786–1795 (2013).
89. Wang, T., Song, X. & Xia, H. H. Equatorial anisotropy in the inner part of Earth's inner core from autocorrelation of earthquake coda. *Nat. Geosci.* **8**, 224–227 (2015).
90. Frost, D. A., Lasbleis, M., Chandler, B. & Romanowicz, B. Dynamic history of the inner core constrained by seismic anisotropy. *Nat. Geosci.* **14**, 531–535 (2021).
91. Beghein, C. & Trampert, J. Robust normal mode constraints on inner-core anisotropy from model space search. *Science* **299**, 552–555 (2003).
92. Phạm, T.-S. & Tkalčić, H. Up-to-fivefold reverberating waves through the Earth's center and distinctly anisotropic innermost inner core. *Nat. Commun.* **14**, 754 (2023).
93. Shearer, P. M. Constraints on inner core anisotropy from PKP(DF) travel times. *J. Geophys. Res. Solid Earth* **99**, 19647–19659 (1994).
94. Su, W. & Dziewonski, A. M. Inner core anisotropy in three dimensions. *J. Geophys. Res. Solid Earth* **100**, 9831–9852 (1995).
95. Song, X. & Helmberger, D. V. Depth dependence of anisotropy of Earth's inner core. *J. Geophys. Res. Solid Earth* **100**, 9805–9816 (1995).
96. Song, X. & Helmberger, D. V. Seismic evidence for an inner core transition zone. *Science* **282**, 924–927 (1998).
97. Souriau, A. & Roudil, P. Attenuation in the uppermost inner core from broad-band GEOSCOPE PKP data. *Geophys. J. Int.* **123**, 572–587 (1995).
98. Durek, J. J. & Romanowicz, B. Inner core anisotropy inferred by direct inversion of normal mode spectra. *Geophys. J. Int.* **139**, 599–622 (1999).
99. Ouzounis, A. & Creager, K. C. Isotropy overlying anisotropy at the top of the inner core. *Geophys. Res. Lett.* **28**, 4331–4334 (2001).
100. Garcia, R. Constraints on upper inner-core structure from waveform inversion of core phases. *Geophys. J. Int.* **150**, 651–664 (2002).
101. Song, X. & Xu, X. Inner core transition zone and anomalous PKP(DF) waveforms from polar paths. *Geophys. Res. Lett.* **29**, 1-1–1-4 (2002).
102. Niu, F. & Wen, L. Seismic anisotropy in the top 400 km of the inner core beneath the "eastern" hemisphere. *Geophys. Res. Lett.* **29**, 53-1–53-5 (2002).
103. Ishii, M. & Dziewoński, A. M. Distinct seismic anisotropy at the centre of the Earth. *Phys. Earth Planet. Inter.* **140**, 203–217 (2003).
104. Li, X. & Cormier, V. F. Frequency-dependent seismic attenuation in the inner core, 1. A viscoelastic interpretation. *J. Geophys. Res. Solid Earth* **107**, ESE 13-1–ESE 13-20 (2002).
105. Cormier, V. F. & Li, X. Frequency-dependent seismic attenuation in the inner core 2. A scattering and fabric interpretation. *J. Geophys. Res. Solid Earth* **107**, ESE 14-1–ESE 14-15 (2002).
106. Stroujkova, A. & Cormier, V. F. Regional variations in the uppermost 100 km of the Earth's inner core. *J. Geophys. Res. Solid Earth* **109**, B10307 (2004).
107. Cormier, V. F. & Stroujkova, A. Waveform search for the innermost inner core. *Earth Planet. Sci. Lett.* **236**, 96–105 (2005).
108. Yu, W. & Wen, L. Complex seismic anisotropy in the top of the Earth's inner core beneath Africa. *J. Geophys. Res. Solid Earth* https://doi.org/10.1029/2006JB004868 (2007).
109. Cao, A. & Romanowicz, B. Test of the innermost inner core models using broadband PKIKP travel time residuals. *Geophys. Res. Lett*. https://doi.org/10.1029/2007GL029384 (2007).
110. Niu, F. & Chen, Q.-F. Seismic evidence for distinct anisotropy in the innermost inner core. *Nat. Geosci.* **1**, 692–696 (2008).
111. Sun, X. & Song, X. The inner inner core of the Earth: texturing of iron crystals from three-dimensional seismic anisotropy. *Earth Planet. Sci. Lett.* **269**, 56–65 (2008).
112. Irving, J. C. E. & Deuss, A. Stratified anisotropic structure at the top of Earth's inner core: a normal mode study. *Phys. Earth Planet. Inter.* **186**, 59–69 (2011).
113. Tanaka, S. Depth extent of hemispherical inner core from PKP(DF) and PKP(Cdiff) for equatorial paths. *Phys. Earth Planet. Inter.* **210**, 50–62 (2012).
114. Waszek, L. & Deuss, A. A low attenuation layer in the Earth's uppermost inner core. *Geophys. J. Int.* **195**, 2005–2015 (2013).
115. Lythgoe, K. H. & Deuss, A. The existence of radial anisotropy in Earth's upper inner core revealed from seismic normal mode observations. *Geophys. Res. Lett.* **42**, 4841–4848 (2015).
116. Frost, D. A. & Romanowicz, B. On the orientation of the fast and slow directions of anisotropy in the deep inner core. *Phys. Earth Planet. Inter.* **286**, 101–110 (2019).
117. Stephenson, J. *Cylindrical Anisotropy of Earth's Inner Core Re-examined Through Robust Parameter Search*. PhD thesis, Australian National Univ. (2020).
118. Bergman, M. I., Agrawal, S., Carter, M. & Macleod-Silberstein, M. Transverse solidification textures in hexagonal close-packed alloys. *J. Cryst. Growth* **255**, 204–211 (2003).
119. Bergman, M. I. Measurements of electric anisotropy due to solidification texturing and the implications for the Earth's inner core. *Nature* **389**, 60–63 (1997).
120. Cottaar, S. & Buffett, B. Convection in the Earth's inner core. *Phys. Earth Planet. Inter.* **198**, 67–78 (2012).
121. Yoshida, S., Sumita, I. & Kumazawa, M. Growth model of the inner core coupled with the outer core dynamics and the resulting elastic anisotropy. *J. Geophys. Res. Solid Earth* **101**, 28085–28103 (1996).
122. Karato, S. Seismic anisotropy of the Earth's inner core resulting from flow induced by Maxwell stresses. *Nature* **402**, 871–873 (1999).
123. Buffett, B. A. & Bloxham, J. Deformation of Earth's inner core by electromagnetic forces. *Geophys. Res. Lett.* **27**, 4001–4004 (2000).

124. Lasbleis, M. & Deguen, R. Building a regime diagram for the Earth's inner core. *Phys. Earth Planet. Inter.* **247**, 80–93 (2015).
125. Deguen, R. & Cardin, P. Tectonic history of the Earth's inner core preserved in its seismic structure. *Nat. Geosci.* **2**, 419–422 (2009).
126. Buffett, B. A. Onset and orientation of convection in the inner core. *Geophys. J. Int.* **179**, 711–719 (2009).
127. Labrosse, S. Thermal and compositional stratification of the inner core. *Comptes Rendus Geosci.* **346**, 119–129 (2014).
128. Deguen, R., Alboussiere, T. & Cardin, P. Thermal convection in Earth's inner core with phase change at its boundary. *Geophys. J. Int.* **194**, 1310–1334 (2013).
129. Pourovskii, L. V., Mravlje, J., Pozzo, M. & Alfe, D. Electronic correlations and transport in iron at Earth's core conditions. *Nat. Commun.* **11**, 4105 (2020).
130. Gubbins, D., Alfe, D. & Davies, C. J. Compositional instability of Earth's solid inner core. *Geophys. Res. Lett.* **40**, 1084–1088 (2013).
131. Aubert, J., Amit, H., Hulot, G. & Olson, P. Thermochemical flows couple the Earth's inner core growth to mantle heterogeneity. *Nature* **454**, 758–761 (2008).
132. Davies, C. J. & Mound, J. E. Mantle-induced temperature anomalies do not reach the inner core boundary. *Geophys. J. Int.* **219**, S21–S32 (2019).
133. Deguen, R., Alboussière, T. & Labrosse, S. Double-diffusive translation of Earth's inner core. *Geophys. J. Int.* **214**, 88–107 (2018).
134. Deguen, R. & Cardin, P. Thermochemical convection in Earth's inner core. *Geophys. J. Int.* **187**, 1101–1118 (2011).
135. Alboussiere, T., Deguen, R. & Melzani, M. Melting-induced stratification above the Earth's inner core due to convective translation. *Nature* **466**, 744–747 (2010).
136. Monnereau, M., Calvet, M., Margerin, L. & Souriau, A. Lopsided growth of Earth's inner core. *Science* **328**, 1014–1017 (2010).
137. Deguen, R., Cardin, P., Merkel, S. & Lebensohn, R. A. Texturing in Earth's inner core due to preferential growth in its equatorial belt. *Phys. Earth Planet. Inter.* **188**, 173–184 (2011).
138. Buffett, B. A. & Wenk, H.-R. Texturing of the Earth's inner core by Maxwell stresses. *Nature* **413**, 60–63 (2001).
139. Deguen, R. Structure and dynamics of Earth's inner core. *Earth Planet. Sci. Lett.* **333**, 211–225 (2012).
140. Deuss, A. Normal mode constraints on shear and compressional wave velocity of the Earth's inner core. *Earth Planet. Sci. Lett.* **268**, 364–375 (2008).
141. Lin, J.-F. et al. Sound velocities of iron-nickel and iron-silicon alloys at high pressures. *Geophys. Res. Lett.* **30**, 2112–2115 (2003).
142. Antonangeli, D. et al. Composition of the Earth's inner core from high-pressure sound velocity measurements in Fe-Ni-Si alloys. *Earth Planet. Sci. Lett.* **295**, 292–296 (2010).
143. Grechnev, G. E., Ahuja, R. & Eriksson, O. Magnetic susceptibility of hcp iron and the seismic anisotropy of Earth's inner core. *Phys. Rev. B* **68**, 64414 (2003).
144. Sun, S. et al. Superionic effect and anisotropic texture in Earth's inner core driven by geomagnetic field. *Nat. Commun.* **14**, 1656 (2023).
145. Aubert, J., Labrosse, S. & Poitou, C. Modelling the palaeo-evolution of the geodynamo. *Geophys. J. Int.* **179**, 1414–1428 (2009).
146. Davies, C. J. et al. Dynamo constraints on the long-term evolution of Earth's magnetic field strength. *Geophys. J. Int.* **228**, 316–336 (2022).
147. Bono, R. K., Tarduno, J. A., Nimmo, F. & Cottrell, R. D. Young inner core inferred from Ediacaran ultra-low geomagnetic field intensity. *Nat. Geosci.* **12**, 143–147 (2019).
148. Zhou, T. et al. Early Cambrian renewal of the geodynamo and the origin of inner core structure. *Nat. Commun.* **13**, 1–7 (2022).
149. Lloyd, S. J., Biggin, A. J., Paterson, G. A. & McCausland, P. J. A. Extremely weak early Cambrian dipole moment similar to Ediacaran: evidence for long-term trends in geomagnetic field behaviour? *Earth Planet. Sci. Lett.* **595**, 117757 (2022).
150. Thallner, D., Biggin, A. J. & Halls, H. C. An extended period of extremely weak geomagnetic field suggested by palaeointensities from the Ediacaran Grenville dykes (SE Canada). *Earth Planet. Sci. Lett.* **568**, 117025 (2021).
151. Lloyd, S. J., Biggin, A. J., Halls, H. & Hill, M. J. First palaeointensity data from the Cryogenian and their potential implications for inner core nucleation age. *Geophys. J. Int.* **226**, 66–77 (2021).
152. Zhang, Y., Swanson-Hysell, N. L., Avery, M. S. & Fu, R. R. High geomagnetic field intensity recorded by anorthosite xenoliths requires a strongly powered late Mesoproterozoic geodynamo. *Proc. Natl Acad. Sci. USA* **119**, e2202875119 (2022).
153. Christensen, U. R. & Aubert, J. Scaling properties of convection-driven dynamos in rotating spherical shells and application to planetary magnetic fields. *Geophys. J. Int.* **166**, 97–114 (2006).
154. Tassin, T., Gastine, T. & Fournier, A. Geomagnetic semblance and dipolar-multipolar transition in top-heavy double-diffusive geodynamo models. *Geophys. J. Int.* **226**, 1897–1919 (2021).
155. Tabazadeh, A., Djikaev, Y. S. & Reiss, H. Surface crystallization of supercooled water in clouds. *Proc. Natl Acad. Sci. USA* **99**, 15873–15878 (2002).

Acknowledgements
A.J.W., A.M.W., D.A., M.P. and C.J.D. acknowledge support from a Natural Environment Research Council (NERC) grant, reference NE/T000228/1. A.J.W. and C.J.D. also acknowledge NERC grant number NE/V010867/1, A.M.W. and C.J.D. acknowledge NERC grant number NE/T004835/1, and D.A. and M.P. acknowledge NERC grant numbers NE/M000990/1 and NE/R000425/1. M.P. acknowledges the funding from the DOME 4.0 project from the European Union's Horizon 2020 Research and Innovation Programme under grant agreement number 953163. A.D. acknowledges support from European Research Council (ERC) under the European Union's Horizon 2020 Research and Innovation Programme (grant agreement number 681535 - ATUNE) and a Vici award number 016.160.310/526 from the Netherlands Organisation for Scientific Research (NWO). The authors thank M. Lasbleis for her helpful discussion on the dynamics of the inner core.

Author contributions
All authors contributed to conceptualization of this Review and the review and editing process of writing the manuscript. A.D. carried out data curation for all seismological evidence used. A.J.W., A.M.W. and C.J.D. previously developed the methodologies, thermal history models and other analytical approaches used to synthesize previous studies in this Review. A.J.W. conducted the formal analysis and writing of the original draft.

Competing interests
The authors declare no competing interests.

Additional information
Supplementary information The online version contains supplementary material available at https://doi.org/10.1038/s43017-024-00639-6.

Peer review information *Nature Reviews Earth & Environment* thanks Renaud Deguen and the other, anonymous, reviewer(s) for their contribution to the peer review of this work.

Publisher's note Springer Nature remains neutral with regard to jurisdictional claims in published maps and institutional affiliations.